International Journal of Pharmaceutics 637 (2023) 122883

Contents lists available at ScienceDirect

International Journal of Pharmaceutics

journal homepage: www.elsevier.com/locate/ijpharm

Supramolecular assemblies based on polymeric cyclodextrin nanosponges and a cationic porphyrin with antimicrobial photodynamic therapy action

Roberto Zagami [a,b,1,*], Alberto Rubin Pedrazzo [c,1], Domenico Franco [b,1], Fabrizio Caldera [c], Laura M. De Plano [b], Mariachiara Trapani [a], Salvatore Patanè [d], Francesco Trotta [c], Antonino Mazzaglia [a,*]

[a] CNR-ISMN, Istituto per lo Studio dei Materiali Nanostrutturati, URT Messina c/o Dipartimento di Scienze Chimiche, Biologiche, Farmaceutiche ed Ambientali, University of Messina, Viale F. Stagno d'Alcontres 31, Messina 98166, Italy
[b] Dipartimento di Scienze Chimiche, Biologiche, Farmaceutiche ed Ambientali, University of Messina, Viale F. Stagno d'Alcontres 31, Messina 98166, Italy
[c] Dipartimento di Chimica, University of Torino, Via Pietro Giuria 7, 10125 Torino, Italy
[d] Dipartimento di Scienze Matematiche e Informatiche, Scienze Fisiche e Scienze della Terra, University of Messina, Viale F. Stagno d'Alcontres, 31, 98166 Messina, Italy

A B S T R A C T

Within of the increasing requirement of alternative approaches to fight emerging infections, nano-photosensitisers (nanoPS) are currently designed with the aim to optimize the antimicrobial photodynamic (aPDT) efficacy. The utilize of less expensive nanocarriers prepared by simple and eco-friendly methodologies and commercial photosensitisers are highly desiderable. In this direction, here we propose a novel nanoassembly composed of water soluble anionic polyester β-CD nanosponges (β-CD-PYRO hereafter named βNS) and the cationic 5,10,15,20-tetrakis(1-methylpyridinium-4- yl)porphine (TMPyP). Nanoassemblies were prepared in ultrapure water by mixing PS and βNS, by exploiting their mutual electrostatic interaction, and characterized by various spectroscopic techniques such as UV/Vis, Steady-State and Time Resolved Fluorescence, Dynamic Light Scattering and ζ-potential. NanoPS produce appreciable amount of single oxygen similar to free porphyrin and a prolonged stability after 6 days of incubations in physiological conditions and following photoirradiation. Antimicrobial photodynamic action against fatal hospital-acquired infections such as *P. aeruginosa* and *S. aureus* was investigated by pointing out the ability of cationic porphyrin loaded- CD nanosponges to photo-kill bacterial cells at prolonged time of incubation and following irradiation (MBC_{99} = 3.75 μM, light dose = 54.82 J/cm^2).

1. Introduction

Nowadays, the search of microbial control strategies is a current challenge to fight emerging infections, by overcoming the multidrug resistance (MDR). In this direction, Antimicrobial Photodynamic Therapy (aPDT) by using smart supramolecular photosensitiser systems showed promising applications (Vera et al., 2021). aPDT relies with the utilize of a photosensitizer (PS) with physico-chemical features able to interact with bacterial membrane and upon irradiation with Vis/near IR light, it produces radical oxygen species (ROS) and in particular singlet oxygen ($^1O_2$), for targeting and killing pathogen agents (Almeida et al., 2020; Shi et al., 2019). Cationic photosensitisers (Klausen et al., 2020; Zheng et al., 2020), among them cationic porphyrins (Oyim et al., 2021), are widely employed against bacterial infections because of their strong electrostatic binding with both Gram (-) and Gram (+) bacterial wall. Their aPDT efficiency depends by features as singlet oxygen production, charge number, charge distribution, aggregation behavior and amphiphilic molecular balance (Simões et al., 2016).

5,10,15,20-Tetrakis(1-methylpyridinium-4-yl)porphyrin (TMPyP) and its metal complexes (Zn^{2+}, Pt^{2+} and Pd^{2+}) was extensively used to enhance antimicrobial photoinactivation of bacterial and fungal strains (Pinto et al., 2021; Seeger et al., 2020).

Photosensitiser nanosystems, so-called nanophotosensitisers (nanoPS), are currently developed to address the drawbacks due the limitation of single photoactive molecules such as the lack of solubility and stability in the biological media, biocompatibility, bioavailability, selectivity in the target tissue and stimuli-responsiveness upon triggers for controlled release of the photodrug (Awad et al., 2022; Youf et al., 2021). A plethora of nanoPS based on polymeric (Judzewitsch et al., 2021; Zhang et al., 2022), lipid (Plenagl et al., 2018), magnetic (Toledo et al., 2020), noble-metals and silica-based nanoparticles (Elashnikov et al., 2019; Wysocka-Król et al., 2018), as well as carbon nanomaterials were recently proposed in combinatory antimicrobial approaches or for their promising applications (Sah et al., 2018; Trapani et al., 2020). Also

* Corresponding authors at: CNR-ISMN, Istituto per lo Studio dei Materiali Nanostrutturati, URT Messina c/o Dipartimento di Scienze Chimiche, Biologiche, Farmaceutiche ed Ambientali, University of Messina, Viale F. Stagno d'Alcontres 31, Messina 98166, Italy.
[1] Equal contributors.

https://doi.org/10.1016/j.ijpharm.2023.122883
Received 19 November 2022; Received in revised form 19 March 2023; Accepted 20 March 2023
Available online 25 March 2023

PSs were entrapped in gel matrixes or cross-linked in nanogels leading to nano-phototheranostic tools (Chambre et al., 2018; Kirar et al., 2019).

Interestingly, in this scenario Wu et al reported pH-responsive photodynamic nanoparticles, fabricated in layer-by layer fashion, for enhanced penetration and antibacterial efficiency in vitro and in vivo (Wu et al., 2021). Therefore, the utilize of anionic nanoPS with both reduced toxicity in healthy tissues and superior permeation in infected sites are highly attractive. Various macrocycles, such as cucurbit- [7]uril anchoring porphyrin for aPDT (Özkan et al., 2019), or by forming host–guest complexes with the cationic porphyrin TMPyP was proposed as bacteria-responsive phototherapeutics (Hu et al., 2022). Cyclodextrins (CDs) are a family of cyclic oligosaccharides with a toroidal structure, composed of α-D-glucopyranose units, able to conjugate (Mineo, 2014) or complex PSs within or outside the cavity by self-assembly, sustaining drug release for improved (photo)therapeutic action (Conte et al., 2014; Galstyan et al., 2016; Ikeda et al., 2017; Zagami et al., 2019). Some of us and other groups reported supramolecular pseudo-spherical nanocomplexes (Zagami et al., 2020) and nanorods (Khurana et al., 2019) based on trade cyclodextrins (CD) with precise stoichiometries for aPDT.

Supramolecular nanoplatforms based on polymeric CDs were commonly used to enhance the complexation ability of antibiotics, photosensitisers and anticancer drugs for combined (photo)theranostic strategies (Fraix et al., 2019; Hada et al., 2022; Tian et al., 2020; Wang et al., 2019). A polymeric CD- based deliver systems grafting the photosensitiser Chlorin e6 (Ce6) that targets bacteria were reported for photodynamic ablation against biofilms and decreased toxicity in model cells (Gao et al., 2019). Furthermore finished -fabric of polymeric CDs entrapping PSs were developed by our group as drug-eluiting covering for surgical infections (Castriciano et al., 2017).

CD Nanosponges (CDNS) are cross-linked CD polymers nanostructured within a three-dimensional network: the reactive hydroxyl groups oriented to the outer side of CDs allows them to act as polyfunctional monomers, permitting to cross-link with a variety of chemical (bi or polyfunctional), such as dianhydrides, diisocyanates, epoxides, carboxylic acids, etc. The cross-linking process of CDs brings benefits to CDNSs if compared to native CDs by increasing the number of complexation sites and forming complexes with different types of lipophilic or hydrophilic molecules. The polarity and dimension of the polymer network can be easily controlled by varying the type and degree of cross-linking, strongly influencing the final features (Trotta, 2011).

The application of NSs has been widely explored in several scientific and technological fields (Alongi et al., 2010) but the one of the main area of investigation and research nowadays concern applications in pharmaceutical and biomedical sciences. CDNS shows biocompatibility, entrapping capability towards numerous drugs, reduced toxicity, and resistance to therapeutics for prospective application in nanodelivery (Caldera et al., 2017; Swaminathan et al., 2016). For instance, in a previous work some of us evaluated the cytotoxicity of nanosponges on human umbilical vein endothelial cells (HUVECs) indicating no cell injury (Appleton et al., 2020).

Within our ongoing research on nanoPS based on cyclodextrin, in this paper we propose a nanoconstruct composed of water dispersible anionic polyester β-CD nanosponges, (β-CD-PYRO hereafter named βNS) and the cationic porphyrin TMPyP (Scheme1). To the best of our knowledge, this is the first CD/porphyrin nanosponge proposed for aPDT. Our βNS/TMPyP nanoassembly combines the properties of anionic carriers, aimed to minimize the intrinsic dark toxicity of cationic nanoPS (Mazzaglia et al., 2017; Sortino et al., 2006), and the well-known photo-antibacterial identity of cationic porphyrins. The novel nanoPS based on photosensitizing CD nanosponges were fully characterized by complementary spectroscopic methods. Moreover newly we investigated how the effect of the photobactericidal action of the cationic porphyrin can be modulated by the presence of β-CD nanosponges for a long-lasting antibacterial effect for future application in the treatment of secondary infections. With this idea in mind, βNS/TMPyP antimicrobial photodynamic action was investigated against bacteria involved in fatal hospital-acquired infections such as *P. aeruginosa* and *S. aureus*, by assessing as the photostability of the nanoassembly can affect the aPDT outcomes in vitro.

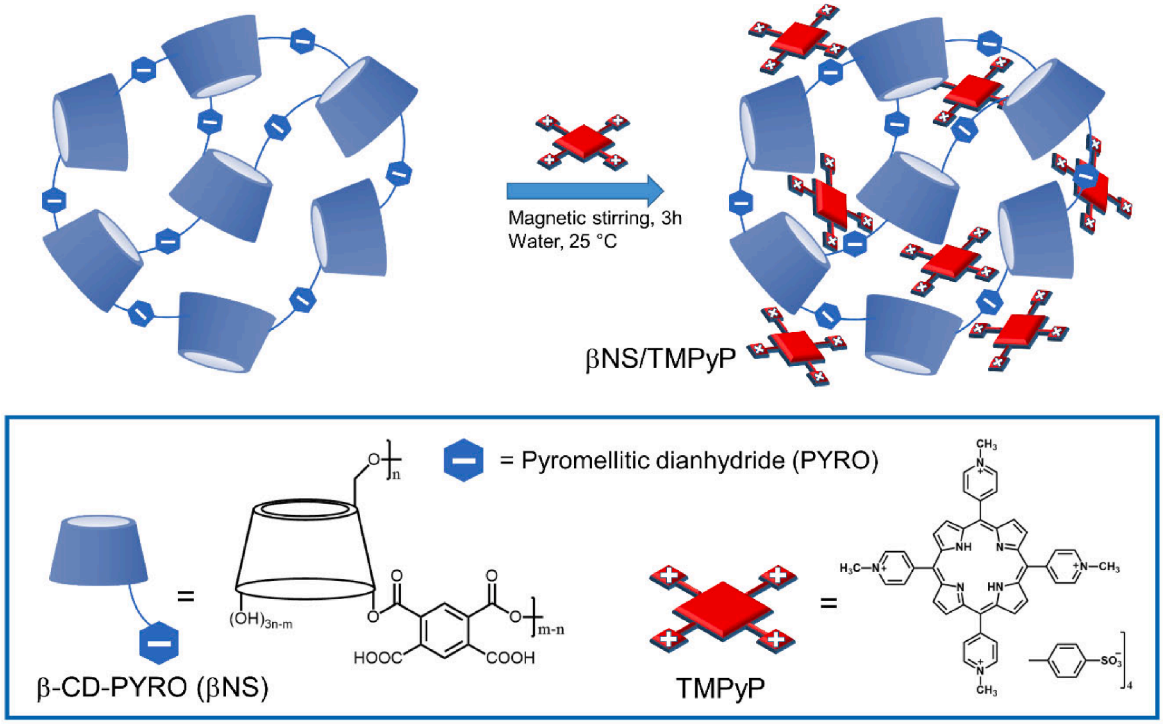

Scheme 1. Sketched view of the proposed NanoPS based on β-CD-PYRO nanosponge (βNS) entrapping the cationic porphyrin TMPyP.

2. Materials and methods

2.1. Materials

2.1.1. General

β-cyclodextrin (β-CD) were kindly provided by Roquette Italia SpA, pyromellitic dianhydride (PYRO), Dimethyl sulfoxide (DMSO)), acetone and ethanol were purchased from Sigma Aldrich (Steinheim, Germany) and used with no further purification. β-CD was dried in oven at 100 °C until constant weight before use.

5,10,15,20-tetrakis(1-methylpyridinium-4-yl)porphine tetrakis(p-toluenesulfonate) (TMPyP, FW = 1363.60) was purchased from Sigma-Aldrich. A stock solution of porphyrin (300 μM) was freshly prepared and stored in the dark. The concentration used in the experiments was calculated by UV/Vis using the molar extinction coefficients at the B-band (TMPyP: 2.34×10^5 M^{-1} cm^{-1}, λ = 422 nm). All the dispersions used for nanoassemblies formation and spectroscopic characterizations were prepared in ultrapure water (Eurospital, Trieste, Italy) or in 10 mM phosphate buffer containing NaCl (137 mM) and KCl (2.7 mM) at pH 7.4 (PBS).

2.1.2. Synthesis of β-CD-PYRO (βNS)

βNS was prepared by slightly modifying an already reported procedure (Rubin Pedrazzo et al., 2019): briefly, 12 g of β-CD was dissolved in 50 mL of DMSO in a 100 mL round bottom flask, under vigorous stirring. After complete solubilization of the β-CD, 6.3 mL of triethylamine (Et_3N) is added. After few minutes, the pyromellitic dianhydride (PYRO) is added at room temperature, at 8:1 PYRO/βCD molar ratio (about 18 g of PYRO). The obtained bulk was crushed, then it was stirred in an excess of water. The suspension is then left to settle, the supernatant is removed and replaced with fresh deionized water. This cycle was repeated until a clear and colorless supernatant was observed. The NS was filtered in a Buchner funnel, using an excess of water and acetone and finally dried at room temperature.

2.1.3. Preparation of βNS/TMPyP nanoassemblies

Nanoassemblies based on βNS and TMPyP (βNS/TMPyP) were obtained dissolving 50 mg of βNS in 10 mL of TMPyP aqueous solution (147 μM, 2 mg). The dispersion at 25:1 βNS/TMPyP mass ratio was kept under magnetic stirring for about 3 h at room temperature (r.t. ≅ 25 °C). βNS/TMPyP was recovered through centrifugation and purified washing for 3 times with H_2O to remove the free porphyrin. The supernatants were collected and analyzed by UV/Vis spectroscopy to determine the amount of unloaded porphyrin. TMPyP actual loading into the nanoassembly was calculated by the difference between starting TMPyP added into formulation and unloaded TMPyP detected in the supernatants. A calibration curve for TMPyP has been built using a solution with a known concentration of porphyrin and, as solvent, the supernatant of a blank βNS dispersion in a range of concentration from 0.5 to 5 μM ($\varepsilon_{\lambda 429nm} = 2.08 \times 10^5 \pm 436$ M^{-1} cm^{-1}).

TMPyP actual loading (AL%), theoretical loading (TL%) and entrapment efficiency percentages (EE%) were evaluated using the following Equations:

$$AL\% = \frac{amount\ of\ TMPyP\ into\ the\ nanoassemblies}{weight\ of\ the\ nanoassemblies} \times 100 \quad (1)$$

$$TL\% = \frac{weight\ of\ TMPyP\ added\ to\ formulation}{weight\ of\ the\ nanoassemblies} \times 100 \quad (2)$$

$$EE\% = \frac{amount\ of\ TMPyP\ into\ the\ nanoassemblies}{weight\ of\ TMPyP\ addedt\ to\ formulation} \times 100 \quad (3)$$

The final dispersion was freeze-dried and a weighed amount was dissolved in water for the characterization.

2.2. Methods

2.2.1. UV/Vis and Steady state and time resolved fluorescence spectroscopy

UV/Vis spectra were acquired on an Agilent model 8453 diode array spectrophotometer using 1 and 0.5 cm path length quartz cells. Steady-state fluorescence measurements were performed on a Jasco model FP-750 spectrofluorimeter. Time resolved fluorescence emission measurements were performed on a Jobin Yvon-Spex Fluoromax 4 spectrofluorimeter using time-correlated single-photon counting technique and a NanoLED (λ = 390 nm) as the excitation source. All the spectra were carried at r.t. ≅ 25 °C or, when it is specified, by controlling temperature by a thermostatic bath.

2.2.2. Size and ζ-Potential of nanoassemblies

Hydrodynamic diameter (D_H) or size, width of distribution (polydispersity index, PDI) and ζ- potential of the βNS/TMPyP nanoassemblies were determined by photon correlation spectroscopy (PCS) by a Zetasizer Nano ZS (Malvern Instrument, Malvern, U.K.) at 25 °C in ultrapure water. The measurements were carried out at 173° angle *vs.* the incident beam at 25 ± 1 °C for each aqueous dispersion. The deconvolution of the correlation curve to an intensity size distribution was obtained by using a non-negative least-squares algorithm. The ζ-potential values were measured using a Zetasizer Nano ZS Malvern Instrument equipped with a He − Ne laser at a power P = 4.0 mW and λ = 633 nm. The results are reported as the mean of three separate measurements on three different batches ± the standard deviation (SD).

2.2.3. Morphological studies by AFM and Microphotoluminescence

Samples were settled according to a microscale preparation as it follows by considering the porphyrin loading equal to 1.2 % w/w: 3.5 mg of βNS were dissolved in 5 mL of a dilute aqueous solution of TMPyP (6 μM, corresponding to the loaded porphyrin, 1.2 % w/w) in a centrifuge tube. The dispersion was vortexed for about 1 min and, after equilibration, it was casted on glass (previously rinsed with ethanol and ultrapure water) and evaporated overnight.

Atomic force microscopy and micro luminescence maps were collected with a NTEGRA by NTMDT equipped with a top visual non-contact silicon cantilever (Zagami et al., 2020). Microphotoluminescence maps were acquired in reflection mode exciting the sample with a solid-state laser operating at 440 nm and focused on the surface through a 100x SLWD objective (Mitutoyo, NA 0,9). The special shape of the tip allows for a simultaneous collection of the morphology and the optical data in the same area as it is possible to focus the laser on the very end of the tip. The system was optically connected with a MS350i spectrometer supplied by SOL and equipped with an ANDOR IDUS CCD. A couple of razor edge filters were plugged into the optical path to filter out the laser photons and allowing the photoluminescence alone to reach the spectrometer and detected by the CCD.

2.2.4. Photodynamic activity and photostability studies

Comparative Singlet-Oxygen Generation Measurements. The amount of produced $^1O_2$ was determined by a standard method based on the bleaching reaction of *p*-nitroso-*N,N'*-dimethylaniline (RNO) (Krishna et al., 1991). The tested sensitizers (TMPyP and βNS/TMPyP, [TMPyP] = 50 μM) were dissolved in ultrapure water with imidazole (10 mM) and RNO (50 μM), so that the absorbance at the excitation wavelength (λ_{exc} = 532 nm) did not exceed the value 0.1, to avoid shielding effects (path length 0.1 cm). Briefly, 5 mL of reaction mixture was placed into a petri dish and exposed to a green-LED homemade apparatus (λ = 532 nm, light irradiance ~ 3.81 mW/cm^2) for different times (from 0 to 30 min) at room temperature. The values of $^1O_2$ quantum yield for a studied system φ_Δ^{system} can be directly obtained from the different slopes (π^{system}) of the rate of bleaching (ΔA_{440} nm *vs* time) by using $\varphi_\Delta^{TMPyP} = 0.74$ (Redmond and Gamlin, 1999) in aqueous solution as a secondary standard according to the following equation:

$$\varphi_{\Delta}^{system} = \varphi_{\Delta}^{TMPyP} \frac{\pi^{system}}{\pi^{TMPyP}} \quad (4)$$

The experiment was carried out in duplicate. Absorbance values were corrected by a multiplicative factor in order to have the same intensity value a t_0 for both TMPyP and βNS/TMPyP (Corrected Absorbance)$_{440nm}$ to get a better comprehension of the comparative measure.

Stability and Photostability of TMPyP and βNS/TMPyP nanoassemblies. Stability studies on TMPyP and βNS/TMPyP were carried out by monitoring the UV/Vis spectral changes and mean D_H values within 6 days in the dark in ultrapure water after storage by thermostatation at T = 25 °C and in PBS at T = 37 °C. In all the experiments TMPyP concentration was 3 μM.

The photostability experiments on TMPyP and βNS/TMPyP were performed on samples dispersed in Mueller Hinton Broth (MHB). Each dispersion was stored in the dark at 37° C for 1 and 6 days and then irradiated for 4 h with a white light-emitting diode (LED) source (light irradiance ~ 3.81 mW/cm^2). In the course of the irradiation, 1200 μL of the samples were collected every hour and analyzed by UV/Vis spectrophotometer. In all the experiments TMPyP concentration was 3.75 μM.

2.2.5. Antimicrobial photodynamic therapy studies.

Bacteria strain, media and growth conditions. *Pseudomonas aeruginosa* ATCC27853 and *Staphylococcus aureus* ATCC29213 were used throughout the experiments. All bacteria strains were purchased from the American Type Culture Collection (LGC Promochem, Milan, Italy) and maintained as 20% glycerol stocks at −80 °C. The strain was cultured in Mueller Hinton Broth (beef infusion solids 2 g/L; Starch 1.5 g/L; casein hydrolysate 17.5 g/L), a liquid medium for antibiotic susceptibility studies.

Minimum Bactericidal Concentration (MBC), established as the concentration able to kill over 99.9% of the microorganisms exposed, was determined increasing aliquots of each specimen, namely TMPyP and TMPyP/NS, ranging between 1.35 and 30 μM. Specifically, a total of 200 μL of semi-exponential cultures, at a final concentration of approximately 10^6 bacteria per mL, was deposited in wells of 96-well plate (4 replicates per condition). Each plate was incubated under a white-light source (26000 lx, irradiance 3.81 mW/cm^2) in gentle shaking (100 rpm, orbital shaker KS-15, Edmund Bühler GmbH) at 37 °C for 4 h (totalling 54.82 J/cm^2 light dose). In order to verify the possible bactericidal activity due to non-irradiated compounds, control plates were prepared in the same conditions but kept in the dark for the entire incubation period. Simultaneously, potential toxicity of βNS alone was simultaneously evaluated until to final concentration of 10 mg/mL.

Bactericidal activity was determined by Colony Forming Unity (CFU) assay and expressed as bacterial viability percentage compared to positive control (CTR, bacterial culture without compounds) (Zagami et al., 2020).

In vitro photostability of βNS/TMPyP was also evaluated for a maximum period of six days. In detail, sterilized TMPyP or βNS/TMPyP, at equal molar concentration to the MBC, and βNS value at the same amount present in the TMPyP-laoded nanoassembly ([TMPyP] = 3.75 μM for free TMPyP and in βNS/TMPyP; βNS = 0.42 mg/mL for free βNS) was incubated in separate 96-well plate (8 replicates per condition) for 1, 2, 4 and 6 days in fresh MHB without bacterial inoculum. After incubation period, a final concentration of approximately 10^5 –10^6 bacteria per mL were inoculated in each condition and irradiated with white LED source (400–700 nm, light irradiance ≅ 3.81 mW/cm^2), at 37 °C for 1, 2 and 4 h corresponding to different light doses, namely about 13.7, 27.4 and 54.8 J/cm^2, respectively. After light exposure, viability of bacteria from each condition was determined by CFU assay. Medium, reagents and tested compounds were evaluated after saturated steam sterilization (121 °C, 20 min). Data were showed as mean ± standard error (SE) and evaluated by one-way analysis of variance followed by a Turkey post-hoc test for multiple comparisons. A p-value of less than 0.05 was considered significant. For each incubation time, 4 independent assays and 4 replicate were performed.

3. Results and discussion

3.1. Synthesis of the β-CD nanosponges

The procedure here reported is slightly modified with respect to the literature, since larger quantities were needed when NSs were employed for water remediation (Rubin Pedrazzo et al., 2019). In the present work the dried samples were ball milled for 30 min at 350 rpm, in order to obtain an homogeneous particle size for all samples of around 200 nm.

3.2. Nanoassemblies formation and interaction studies

Nanoassemblies based on TMPyP loaded-βNS (βNS/TMPyP) were prepared by a one-pot reaction between a known amount of CD nanosponge with an aqueous solution of porphyrin at 25:1 mass ratio. The resulting dispersion leads to a stable supramolecular construct (Scheme 1) whose structure is mainly stabilized by electrostatic interactions acting between the anionic carboxylate groups of the βNS and the positive 1-methylpyridyl rings of the porphyrins. The final dispersion was freeze-dried and a weighed amount was dissolved in water for the technological characterization. An actual loading of 1.2% and an entrapment efficiency of 31.6% were estimated. Despite the CD excess used, porphyrin was only partially entrapped in the core of the nanosponge likely due the weak interaction with CD cavity. In contrast, a high value of EE% had been obtained in βNS loaded with other drugs included in CD cavity (Trotta et al., 2016).

The colloidal behavior of the nanoassemblies was investigated in aqueous solution measuring their size and ζ-potential (Fig. 1).

DLS analysis of the βNS shows a size distribution characterized by the presence of two families of nanoassemblies with a mean size (mean hydrodynamic diameter, mean D_H) of ~ 200 nm and ~ 30 nm with amplitudes of 81% and 19%, respectively. Only a moderate increase was observed for the size of larger aggregates of βNS/TMPyP with mean D_H of ~ 250 nm (71 %) and ~ 20 nm (29 %). Moreover, PDI values pointed out to a certain heterogeneity of the investigated nanoassemblies. This behaviour could be ascribed to the itself nature of βNS which can form, besides that the smallest nanoassemblies of about 200 nm, larger nanosponge aggregates (see morphology studies below). Both the dispersions exhibit a negative ζ-potential with values equal to −36 mV and −49 mV for βNS and βNS/TMPyP, respectively. Surprisingly, ζ is more negative for βNS/TMPyP *vs* βNS although in our experimental conditions the TMPyP is present as tetracationic species. The increase of the

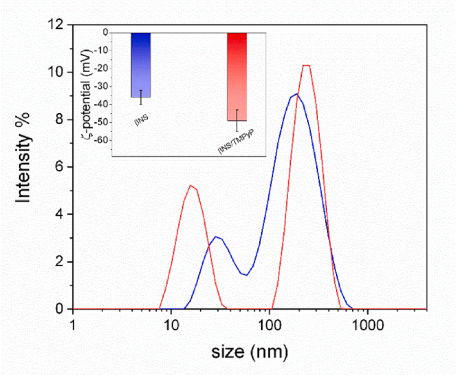

Fig. 1. Size (or D_H) distribution of βNS (blue line) and βNS /TMPyP (red line). In the inset ζ potential ± SD of βNS (blue bar, 5 mg/mL) and βNS/TMPyP (red bar; βNS = 0.7 mg, [TMPyP] = 6 μM), in ultrapure water at 25 °C. (For interpretation of the references to colour in this figure legend, the reader is referred to the web version of this article.)

stability of βNS/TMPyP was plausibly ascribed to the presence of a large excess of βNS which remains mostly uncomplexed at external surface of the nanossemblies. Moreover, the significant excess of carboxylate groups of the nanosponges could take inside the cationic porphyrin which is not covalently embedded into the nanoassemblies. Properties of the nanoassemblies are reported in Table 1.

UV/Vis and fluorescence emission were carried out to get insights into the interaction of the TMPyP in βNS carrier. UV/Vis spectrum of TMPyP in aqueous solution exhibits a very intense B-band centered at 422 nm, accompanied by four Q-bands of much lower intensity at longer wavelengths (λ = 519, 555, 585 and 641 nm). In βNS/TMPyP nanoassemblies, the B-Band undergoes a bathochromic shift of 6 nm and slight hypochromicity compared to TMPyP (Fig. 2a). Moreover, as shown in Figure S1, UV/Vis spectra of freshly prepared βNS/TMPyP in PBS did not essentially change with respect to the systems prepared in ultrapure water, except that for a broadening of the peculiar bands likely due to the ionic strength effect.

The corresponding steady-state emission spectrum of TMPyP in water, shown in Fig. 2b, displays two broad bands at 672 and 713 nm of nearly similar intensity. In βNS/TMPyP the emission profile shows two bands centered at 657 and 719 nm with a higher fluorescence intensity, and a sharper profile compared to free TMPyP in water (Fig. 2b). These spectroscopic features were attributed to intramolecular charge transfer between the peripheral N-methylpyridinium moieties and the center of the TMPyP porphyrin (Mohanty et al., 2008). Moreover, an additional weak band centered at 622 nm was detected and ascribed to the likely formation of TMPyP zinc(II) metal complex. Zinc derivatives of porphyrins are widely studied (Occhiuto et al., 2020). The unwanted formation of small amount of metal derivative is in agreement with results reported recently in literature in which under neutral conditions aqueous porphyrin solutions are able to extract zinc(II) cations that are embedded in the surface of glass or silica where it is present as additive (Romeo et al., 2017). The presence of zinc(II) metal complex was verified acquiring excitation spectra with λ_{em} at 622 nm and 657 nm (Fig. 2c). Whereas excitation spectrum acquired at λ_{em} = 622 nm confirmed the presence of a band centered at 443 nm ascribed to ZnTMPyP complexed into the nanoassemblies, a band centered at 428 nm can be detectable by using λ_{em} at 657 nm pointing out the presence of unmetalated TMPyP loaded within nanosponges. The influence of βNS on the excited state features of TMPyP are highlighted by changes in its excited state lifetime. Time resolved fluorescence lifetime measurements were performed on solutions of TMPyP and βNS/TMPyP nanoassemblies in water (Fig. 3).

Fluorescence time-decay of free TMPyP is well-fitted by monoexponential profile estimating a fluorescence lifetime value of 5.4 ns according to literature data (Santiago et al., 2008). In the nanoassemblies, the decay profile of TMPyP exhibits a biexponential behavior that allows to estimate two fluorescence lifetime of $\tau_1 \cong 2$ ns and $\tau_1 \cong 12$ ns. The shorter one, with a distribution amplitude of 6 %, can be likely identify the presence of small amount of the zinc(II) metal derivative. Whereas, the long-living emitting species, with a greater distribution amplitude (94 %), suggesting the embedding of TMPyP into the colloidal nanoassembly which contributes to the reduction of the nonradiative decay pathways shielding the fluorophore from the solvent interactions (Table 2). This finding is in agreement with TMPyP porphyrins entangled in cyclodextrin nanoaggregates (Zagami et al., 2020) and values reported in literature also evidenced in micellar systems (Gonçalves et al., 2011) or associated in phospholipid vesicles (de Sousa Neto and Tabak, 2012). This effect is remarkable by considering that often, in the presence of chemical species or in metal nanoparticles based nanoassemblies, the quenching of fluorophores emission or the formation of less emissive species are observed (Cordaro et al., 2014; Trapani et al., 2017).

3.3. Morphological studies by AFM and Microphotoluminescence

The morphology acquired by AFM working in tapping mode (Fig. 4a and 4c) highlights the presence of many sponges-like structures with different shape and size, typically ranging between some hundreds of nanometers and one micron (Fig. 4b). As shown in Fig. 4c and 4d, almost all the structures are capable of photoluminescence at wavelengths around 620 nm. The largest are immediately distinguishable in the photoluminescence map, while the smallest are not noticeable as the attainable photoluminescence lateral resolution is diffraction limited.

3.4. Comparative Singlet-Oxygen generated Measurements, stability and photostability studies

The photodynamic potential of βNS/TMPyP was evaluated by typical indirect detection of $^1O_2$ generation. For this experiment, aqueous dispersions of TMPyP and TMPyP-loaded βNS with a concentration of 50 μM for both samples were used to produce a detectable $^1O_2$ amount. The relative rates of singlet oxygen production were obtained comparing the kinetics of RNO degradation obtained with the βNS/TMPyP and with TMPyP as the reference molecule (Fig. 5). The investigated sample generates appreciable amounts of $^1O_2$ ($\varphi\Delta$ βNS/TMPyP = 0.67), in comparison with free TMPyP ($\varphi\Delta$ TMPyP = 0.74). In this situation, the presence of small amount of Zn (II) complexes (≅ 6%) should not affect the photodynamic potential of nanosponges/porphyrin system by considering the similar values of $\varphi\Delta$ βNS/TMPyP and $\varphi\Delta$ Zn(II) TMPyP (equal to 0.88) (Redmond and Gamlin, 1999).

Stability studies were carried out by monitoring the UV/vis spectral changes and mean D_H values within 6 days in the dark in superpure water and in PBS to mimic the physiological conditions. As shown in the figure below (Fig. 6), the position of the peculiar Soret band remains unaltered, showing only a slight decrease *vs* time both for nanoassemblies dispersed after storage at 25 °C in ultrapure water (Fig. 6a) and in PBS at 37 °C (Fig. 6b). In addition, the size of the nanoassemblies

Table 1
Overall properties of βNS[a] and βNS/TMPyP[a]: mean Hydrodynamic Diameter (D_H) or mean size, polidispersity index (PDI) and ζ-potential values, theoretical, actual loading and entrapment efficiency (EE%) in ultrapure water and in PBS 10 mM.

System	Mean D_H (nm ± SD)[b] (%)[c]	PDI	ζ-potential (mV ± SD)	Theoretical Loading %	Actual loading %[e]	EE%[f]
βNS	202 ± 40 (81) 33 ± 11 (19)	0.39 0.33	−36 ± 4	–	–	–
βNS/TMPyP	248 ± 50 (71) 17 ± 3 (29) [255 ± 31 (87%), 21 ± 2 (13%)][d]	≥ 0.4 0.36	−49 ± 6	3.8	1.2	31.6

[a] βNS (average size measured on samples at concentration of 0.7 and 5 mg/mL, pH ≅ 3.20); βNS/TMPyP (0.7 mg/mL, [TMPyP] = 6 μM, pH ≅ 3.64).
[b] SD was calculated on three different batches.
[c] Mean size with corresponding intensity % distribution (only main populations).
[d] in the bracket mean D_H in PBS 10 mM (βNS/TMPyP: 0.7 mg/mL, [TMPyP] = 6 μM, pH ≅ 7).
[e] Actual loading is expressed as the amount of TMPyP (mg) encapsulated per 100 mg of nanoassembly.
[f] Ratio between actual and theoretical loading × 100.

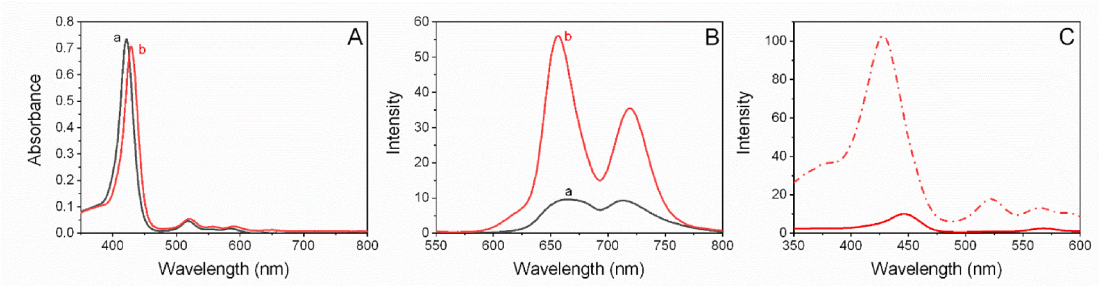

Fig. 2. UV/Vis (A), fluorescence emission (λ_{exc} = 448 nm) (B) of TMPyP (black line, trace a) and βNS/TMPyP (red line, trace b) in ultrapure water and excitation spectra (C) at different emission wavelengths, λ_{em} = 622 nm (red solid line) and λ_{em} = 657 nm (red dash-dot line); [TMPyP] = 3 μM, path length = 1 cm, r.t. (For interpretation of the references to colour in this figure legend, the reader is referred to the web version of this article.)

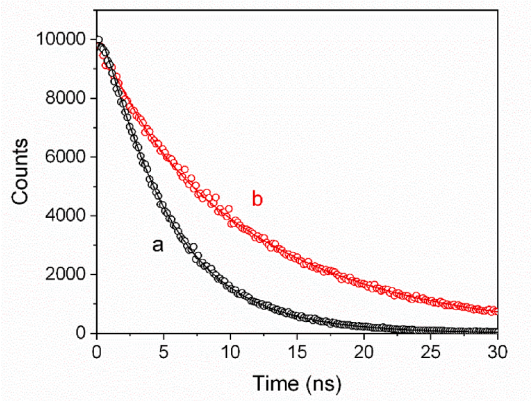

Fig. 3. Time resolved fluorescence decays of TMPyP (a, black circles) and βNS/TMPyP (b, red circles) in ultrapure water; [TMPyP] = 3 μM, λ_{exc} = 390 nm, path length = 1 cm, r.t. (For interpretation of the references to colour in this figure legend, the reader is referred to the web version of this article.)

Table 2
Fluorescence lifetimes of TMPyP and βNS/TMPyP in ultrapure water.

System	$\tau_1 \pm$ SD (ns)[a]	$\tau_2 \pm$ SD (ns)[a]	A_1(%)	A_2(%)
TMPyP	5.4 ± 0.1	–	100	–
βNS/TMPyP	1.8 ± 0.1	11.9 ± 0.2	6	94

[a] Fluorescence lifetimes were measured at λ_{exc} = 390 nm and λ_{em} = 654 nm. A_i is the amplitude of the intensity decay. [TMPyP] = 3 μM, r.t.

remains unchanged until two days (not shown), and the D_H increases after 6 days from about 250 nm to about 400 nm in water and to about 350 nm in PBS (Fig. S2). Therefore, we could assess that no significant aggregation phenomena of the constituent porphyrin chromophores were occurred within a week in conditions mimicking the physiological conditions.

The photostability of TMPyP and βNS/TMPyP was evaluated in aqueous dispersions under the same conditions used for in vitro experiments (fresh MHB, 1 and 6 days incubation with 4 h of irradiation, see Fig. 7). Figure S3 shows the comparison between UV/Vis of freshly prepared dispersion of TMPyP and βNS/TMPyP in MHB (before irradiation at t = 0). In all the cases, B band of porphyrins in MHB is batochromically shifted and undergoes to hypochromicity, except for TMPyP after 6 days. These data suggests that both TMPyP and βNS/TMPyP (before irradiation) strongly interacts with MHB plausibly due to the Zn (II) complexation and interaction with protein of the MHB exhibiting different spectroscopic profiles. By looking at Fig. 7, TMPyP-loaded βNS exhibits a higher photostability compared to the unloaded TMPyP. Photostability of βNS/TMPyP is 68 % and 87 % *vs* 52 % and 73 % of TMPyP for 1 day and 6 days of incubation, respectively. Anyway, the dispersions of the samples incubated for only 1 day are less photostable with respect the dispersions incubated for a longer time (6 days). For this reason we are incline to think that nanosponges could exert mainly a role in the protection of TMPyP from photodegradation rather than modulate the release along the time of the treatment.

3.5. Photobactericidal activity

The photobactericidal activity of both compounds, namely TMPyP and βNS/TMPyP, has been established through biological assays against *P. aeruginosa* and *S. aureus*, among the most common pathogens involved in a wide range of infections, including severe and often fatal hospital-acquired infections, especially in immunocompromised hosts.

For both bacteria, data show a total reduction of the bacterial load both for TMPyP and βNS/TMPyP at TMPyP molar concentration of 3.75 μM, while only *P. aeruginosa* shows a susceptibility for free βNS at concentration of 10 mg/ml. Therefore, in the first analysis it could be asserted that the presence of βNS did not affect the bactericidal activity of the TMPyP. No significant bactericidal activity has been observed for the same conditions without white-light irradiation. In order to investigate if the photostability of TMPyP-loaded nanosponges can affect the aPDT action *vs* time, photobactericidal activity of βNS/TMPyP was evaluated at MBC value molar concentrations after several incubation time in fresh MHB without bacterial inoculums (1, 2, 4 and 6 days) and at several exposition time (Fig. 8), using TMPyP and βNS as positive and negative control, respectively.

Results show a similar bactericidal trend for TMPyP and βNS at all incubation times for both tested bacteria. Specifically, TMPyP induced a total reduction of viable bacteria after 1 h of exposure to light (13.71 J/cm^2), while βNS was non-toxic in accordance with the findings of MBC assay (see Table 3). Otherwise, when TMPyP was complexed with βNS (βNS/TMPyP), the photobactericidal activity was significantly slowed down, so that an exposure of about 4 h of exposure to light (54.82 J/cm^2) was necessary for the complete reduction of the bacterial load. About *S. aureus,* we observe a non-significant reduction after 1 h of exposure, while a 90% reduction after 2 h of exposure at all incubation times, i.e. 1, 2, 4 and 6 days. These findings would indicate that the nanocomplex is highly stable for up to 6 days under physiological conditions. Similar results were obtained also for *P. aeruginosa* at 4 and 6 days of incubation, while after 1 and 2 days of incubation the effect was interestingly improved. It is known that β-cyclodextrin nanosponges have antimicrobial activity when used in the form of drug-free agents against both Gram-positive and Gram-negative (Desai and Shende, 2021). Specifically, it has been suggested that outer membrane in Gram-negative are most susceptible sites to action of cyclodextrins and antimicrobial activity could be due to interruption of the bioprocesses occurring on them (Desai and Shende, 2021). Barnaby et al found that a reduced growth of *P. aeruginosa* ascribable to rupture of the outer membrane vesicles and destruction of lipid rafts was observed (Barnaby et al., 2018). In our in vitro studies, we observed an antimicrobial

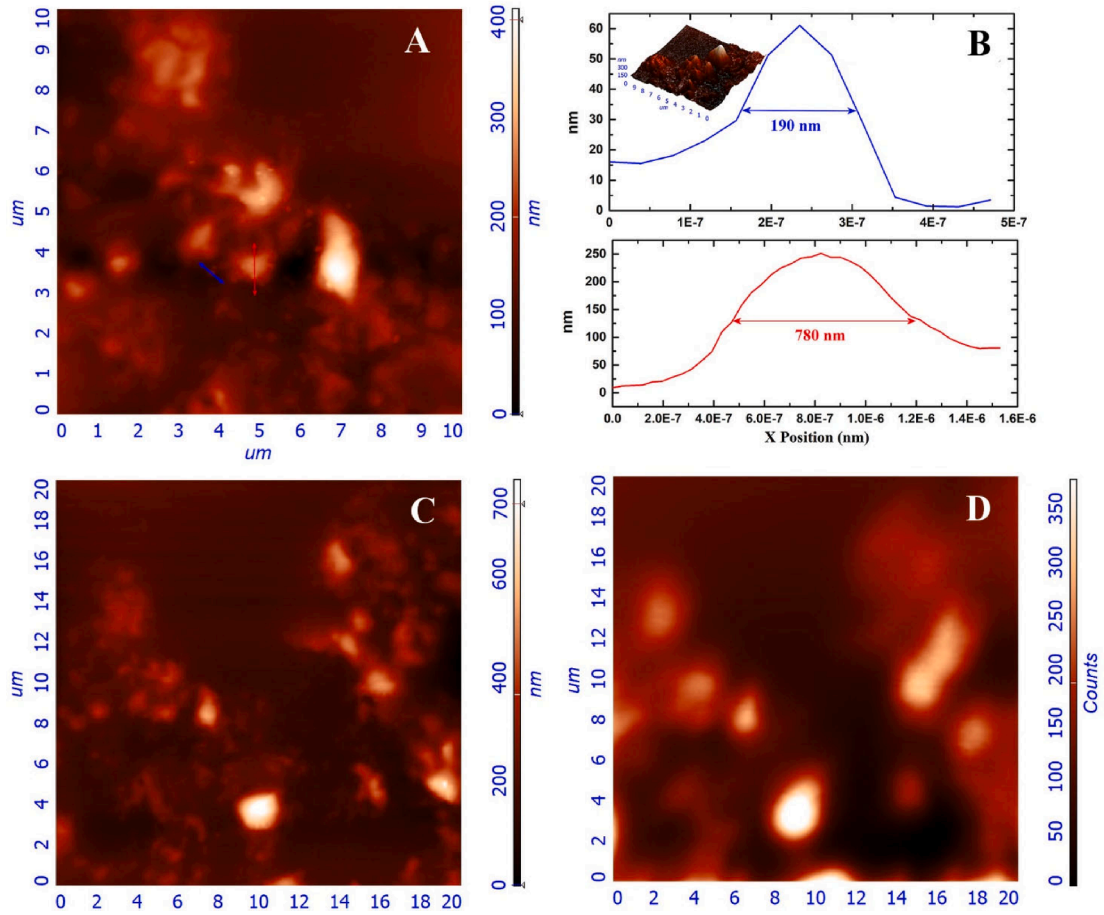

Fig. 4. AFM working in tapping mode on the βNS/TMPyP over an area of 10x 10 μm(A) and 20x20 μm (C). Line profiles acquired along the two double arrows tracked in A with tridimensional profile of A (B). Microphotoluminescence measurements acquired in reflection mode on the area C by exciting the sample at 440 nm (D). All the samples were casted on rinsed glass surfaces (see Experimental Part).

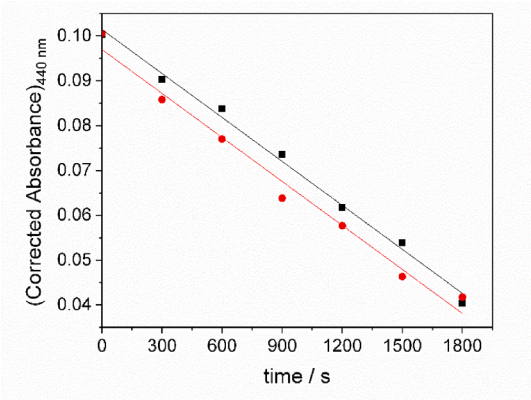

Fig. 5. RNO bleaching kinetics (by following Absorbance at 440 nm) of TMPyP (black squares) and βNS/TMPyP (red circles). Experimental conditions: [TMPyP] = 50 μM in free TMPyP and in βNS/TMPyP, path length = 0.1 cm, r.t.. Absorbance values were corrected by a multiplicative factor in order to get a better visualization. (For interpretation of the references to colour in this figure legend, the reader is referred to the web version of this article.)

activity for βNS alone at 10 mg/mL for *P. aeruginosa*, while no significant activity was found at lower concentrations and against *S. aureus* at all tested concentrations. In the specific case of *P. aeruginosa*, the antimicrobial tests show a better performance after short incubation times (1 and 2 days) compared to longer incubation times (4 and 6 days), hypothesizing, in the first case, a synergistic effect of antibacterial activity due to both βNS and the photoactivated porphyrin after 2 days of incubation time. Otherwise, longer incubation times could reduce the antibacterial effect of βNS, making the bactericidal trend of βNS/TMPyP similar to that observed for Gram-positve strain (*S. aureus*). Therefore, even if nanocomplexes have the same efficiency of the TMPyP alone, in terms of concentration, namely 3.75 μM (see Table 3), they need higher light dose to carry out their aPDT action, confirming the prolonged stability in physiological conditions (about 6 days) that allows to protect porphyrins from photodegradation, preserving photodynamic efficacy *vs* time. These findings suggest a potential use of TMPyP/βNS nanocomplex as modulable nanophotosensitiser and potentially promising for targeted antimicrobial photodynamic therapy in infected wounds.

4. Conclusions

Supramolecular assemblies based on polyester β-CD nanosponges βCD-PYRO and the cationic porphyrin TMPyP form in aqueous medium nanoconstructs with antimicrobial phototherapeutic action. TMPyP interacts within the β-CD nanosponges network by electrostatic linkages and is entrapped mostly as monomer with scarce tendency to form porphyrin supramolecular aggregates. βNS/TMPyP nanoassemblies show a higher emission fluorescence *vs* TMPyP, produce an appreciable amount of singlet oxygen quantum yield similar to free porphyrin and exhibit an higher photostability at different time of treatment in physiological conditions. Moreover, no significant leakage of porphyrin from nanoassemblies was observed in medium mimicking physiological conditions. The highest photostability of βNS/TMPyP is likely

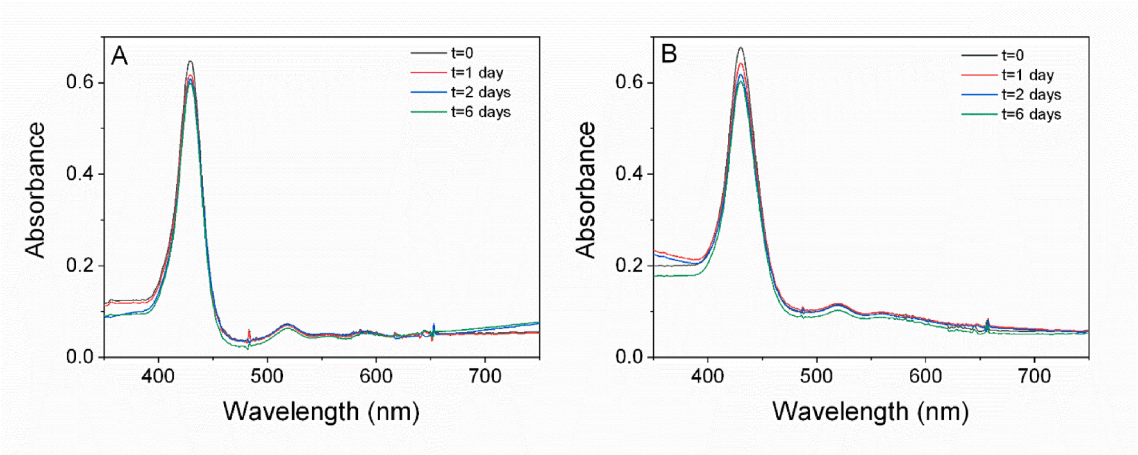

Fig. 6. Stability studies by UV/Vis spectroscopy of β-NS/TMPyP in ultrapure water at 25 °C (A) and PBS at 37 °C (B) *vs* time. In all the dispersion TMPyP concentration was 3 μM, path length = 1 cm.

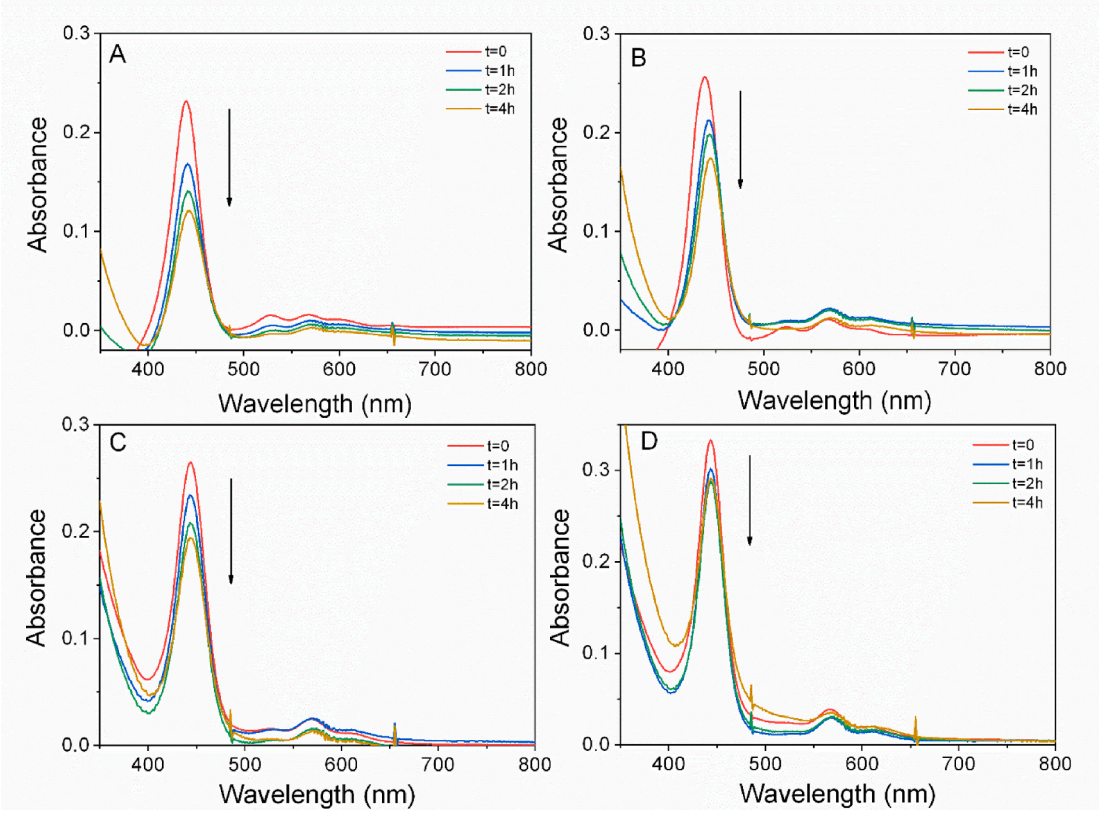

Fig. 7. Photostability studies by UV/Vis spectroscopy of free TMPyP and βNS/TMPyP in MHB stored in the dark at 37 °C for 1 day (A, B) and for 6 days (C, D) and then irradiated with a white-LED source (light irradiance ≅ 3.81 mW/cm^2) for 4 h (light dose: 54.82 J/cm^2). TMPyP concentration was 3.75 μM in all the dispersions, path length = 0.5 cm.

responsible to a lower photobactericidal activity of βNS/TMPyP on both *S. aureus* and *P. aeruginosa* with respect to free TMPyP, even if within the nanocomplex, βNS seem to protect cationic porphyrin by photodegradation. This would allow to have a bactericidal effect also for secondary infections, which could occur during or after treatment of a primary infection, by disadvantaging the onset of resistant strains. In addition, for *P. aeruginosa* a combinatorial effect was observed due to the action of both βNS and TMPyP both upon irradiation, when nanoassemblies were incubated for 1 and 2 days before bacteria inoculum. Altogether, our nanoassemblies composed by β-CD nanosponges and cationic porphyrin could fit the proper compromise between protection of the porphyrins from photodegradation and an efficient photodynamic action in the infected site, plausibly pointing out to a modulated effect of the photobactericidal action of the cationic porphyrin in the presence of cyclodextrin nanosponges. For these reasons these systems can be proposed as promising nanophotosensitisers with tunable properties for future applications in targeted aPDT.

CRediT authorship contribution statement

Roberto Zagami: Data curation, Writing – original draft, Visualization. **Alberto Rubin Pedrazzo:** Data curation, Writing – review &

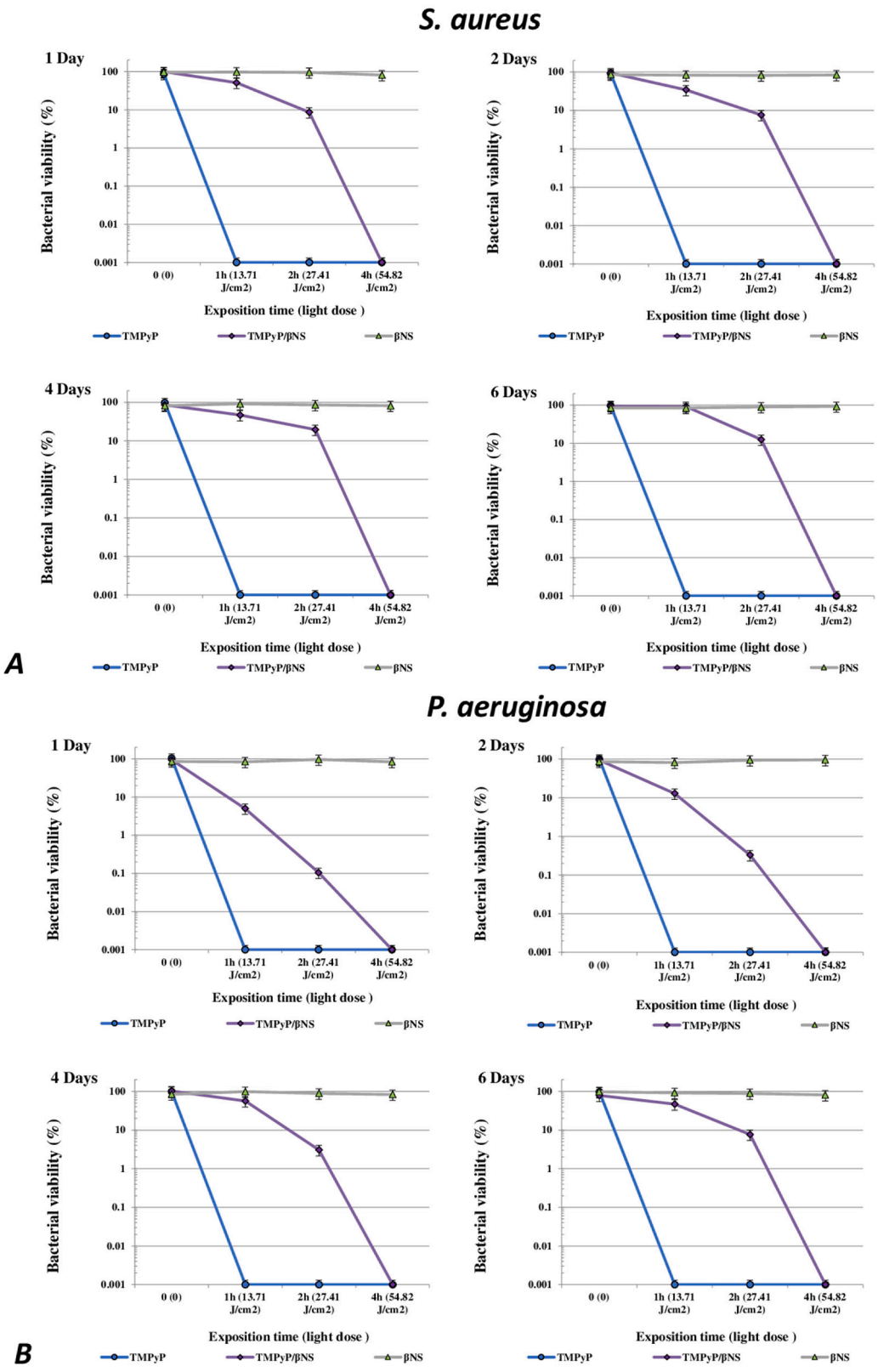

Fig. 8. Photobactericidal activity of βNS/TMPyP against *S. aureus* (A) and *P. aeruginosa* (B) after in vitro release compared to free TMPyP and βNS ([TMPyP] = 3.75 μM for free TMPyP and in βNS/TMPyP; βNS = 0.42 mg/mL in free βNS). For each incubation time, compounds have been incubated for several days (1, 2, 4 and 6 day), before bacteria inoculum (10^5 –10^6 bacteria per mL). 96-well plate was irradiated with a white-LED source with a light irradiance ≅ 3.81 mW/cm^2, immediately after bacterial strain inoculum for different exposition time 1, 2 and 4 h (corresponding to 13.7, 27.4 and 54.8 J/cm^2, respectively). The bacterial viability is determined by CFU assay, and the survival rate expressed as percentage, comparing CFU from each condition to that from positive control without systems (CTR). Tukey's multiple comparisons test has been performed for comparison results from each condition and reported in supplementary materials section(see Tables S1-S8).

Table 3
MBC (μM) against *P. aeruginosa* and *S. aureus* under two different conditions at 37 °C, namely 4 h of White-Light Irradiation (light dose 54.82 J/cm^2) and in the dark.

[a]System	*P. aeruginosa*		*S. aureus*	
	MBC		MBC	
	light	dark	light	dark
[a]βNS	10 mg/mL	10 mg/mL	–	–
[b]TMPyP	3.75 μM	–	3.75 μM	–
[b]βNS/TMPyP	3.75 μM	–	3.75 μM	–

The dashes correspond to a lack of activity below this concentration.
[a] The highest concentration carried out was 10 mg/mL for free βNS.
[b] 30 μM for free and complexed TMPyP.

editing. **Domenico Franco:** Data curation, Writing – original draft, Writing – review & editing. **Fabrizio Caldera:** Writing – review & editing. **Laura M. De Plano:** Data curation, Writing – review & editing, Visualization. **Mariachiara Trapani:** Writing – review & editing, Visualization. **Salvatore Patanè:** Data curation. **Francesco Trotta:** Validation, Writing – review & editing, Funding acquisition. **Antonino Mazzaglia:** Conceptualization, Writing – original draft, Writing – review & editing, Funding acquisition, Supervision.

Declaration of Competing Interest

The authors declare that they have no known competing financial interests or personal relationships that could have appeared to influence the work reported in this paper.

Data availability

The data that has been used is confidential.

Acknowledgments

This work has been partially supported by PON03PE_00216_1 Drug Delivery and partially by European Union (NextGeneration EU), through the MUR-PNRR project SAMOTHRACE (ECS00000022).

Appendix A. Supplementary material

Supplementary data to this article can be found online at https://doi.org/10.1016/j.ijpharm.2023.122883.

References

Almeida, A., Faustino, M.A.F., Neves, M.G.P.M.S., 2020. Antimicrobial photodynamic therapy in the control of covid-19. Antibiotics 9 (6), 320.
Alongi, J., Pošković, M., Frache, A., Trotta, F., 2010. Novel flame retardants containing cyclodextrin nanosponges and phosphorus compounds to enhance eva combustion properties. Polym. Degrad. Stab. 95, 2093–2100. https://doi.org/10.1016/j.polymdegradstab.2010.06.030.
Appleton, S.L., Tannous, M., Argenziano, M., Muntoni, E., Rosa, A.C., Rossi, D., Caldera, F., Scomparin, A., Trotta, F., Cavalli, R., 2020. Nanosponges as protein delivery systems: Insulin, a case study. Int. J. Pharm. 590, 119888 https://doi.org/10.1016/j.ijpharm.2020.119888.
Awad, M., Thomas, N., Barnes, T.J., Prestidge, C.A., 2022. Nanomaterials enabling clinical translation of antimicrobial photodynamic therapy. J. Controlled Release 346, 300–316. https://doi.org/10.1016/j.jconrel.2022.04.035.
Barnaby, R., Koeppen, K., Stanton, B.A., 2018. Cyclodextrins reduce the ability of pseudomonas aeruginosa outer-membrane vesicles to reduce cftr cl− secretion. Am. J. Physiol. Lung Cell Mol. Physiol. 316, L206–L215. https://doi.org/10.1152/ajplung.00316.2018.
Caldera, F., Tannous, M., Cavalli, R., Zanetti, M., Trotta, F., 2017. Evolution of cyclodextrin nanosponges. Int. J. Pharm. 531, 470–479. https://doi.org/10.1016/j.ijpharm.2017.06.072.
Castriciano, M.A., Zagami, R., Casaletto, M.P., Martel, B., Trapani, M., Romeo, A., Villari, V., Sciortino, M.T., Grasso, L., Guglielmino, S., Scolaro, L.M., Mazzaglia, A., 2017. Poly(carboxylic acid)-cyclodextrin/anionic porphyrin finished fabrics as photosensitizer releasers for antimicrobial photodynamic therapy. Biomacromolecules 18, 1134–1144. https://doi.org/10.1021/acs.biomac.6b01752.
Chambre, L., Saw, W.S., Ekineker, G., Kiew, L.V., Chong, W.Y., Lee, H.B., Chung, L.Y., Bretonnière, Y., Dumoulin, F., Sanyal, A., 2018. Surfactant-free direct access to porphyrin-cross-linked nanogels for photodynamic and photothermal therapy. Bioconjugate Chem. 29, 4149–4159. https://doi.org/10.1021/acs.bioconjchem.8b00787.
Conte, C., Scala, A., Siracusano, G., Leone, N., Patanè, S., Ungaro, F., Miro, A., Sciortino, M.T., Quaglia, F., Mazzaglia, A., 2014. Nanoassembly of an amphiphilic cyclodextrin and zn(ii)-phthalocyanine with the potential for photodynamic therapy of cancer. RSC Adv. 4, 43903–43911. https://doi.org/10.1039/C4RA07847K.
Cordaro, M., Mineo, P., Nastasi, F., Magazzù, G., 2014. Facile synthesis of boronic acids on a bodipy core with promising sensitivity towards polyols. RSC Adv. 4, 43931–43933. https://doi.org/10.1039/C4RA08213C.
de Sousa Neto, D., Tabak, M., 2012. Interaction of the meso-tetrakis (4-n-methylpyridyl) porphyrin with gel and liquid state phospholipid vesicles. J. Colloid Interface Sci. 381, 73–82. https://doi.org/10.1016/j.jcis.2012.05.041.
Desai, D., Shende, P., 2021. Drug-free cyclodextrin-based nanosponges for antimicrobial activity. J. Pharm. Innov. 16, 258–268. https://doi.org/10.1007/s12247-020-09442-4.
Elashnikov, R., Radocha, M., Panov, I., Rimpelova, S., Ulbrich, P., Michalcova, A., Svorcik, V., Lyutakov, O., 2019. Porphyrin-silver nanoparticles hybrids: Synthesis, characterization and antibacterial activity. Mater. Sci. Eng. C 102, 192–199. https://doi.org/10.1016/j.msec.2019.04.029.
Fraix, A., Kirejev, V., Malanga, M., Fenyvesi, É., Béni, S., Ericson, M.B., Sortino, S., 2019. A three-color fluorescent supramolecular nanoassembly of phototherapeutics activable by two-photon excitation with near-infrared light. Chem. – Eur. J. 25, 7091–7095. https://doi.org/10.1002/chem.201900917.
Galstyan, A., Kauscher, U., Block, D., Ravoo, B.J., Strassert, C.A., 2016. Silicon(iv) phthalocyanine-decorated cyclodextrin vesicles as a self-assembled phototherapeutic agent against mrsa. ACS Appl. Mater. Interf. 8, 12631–12637. https://doi.org/10.1021/acsami.6b02132.
Gao, Y., Wang, J., Hu, D., Deng, Y., Chen, T., Jin, Q., Ji, J., 2019. Bacteria-targeted supramolecular photosensitizer delivery vehicles for photodynamic ablation against biofilms. Macromol. Rapid Commun. 40 (4), 1800763.
Gonçalves, P.J., Franzen, P.L., Correa, D.S., Almeida, L.M., Takara, M., Ito, A.S., Zílio, S. C., Borissevitch, I.E., 2011. Effects of environment on the photophysical characteristics of mesotetrakis methylpyridiniumyl porphyrin (tmpyp). Spectrochim. Acta A Mol. Biomol. Spectrosc. 79, 1532–1539. https://doi.org/10.1016/j.saa.2011.05.012.
Hada, A.-M., Potara, M., Astilean, S., Cordaro, A., Neri, G., Malanga, M., Nostro, A., Mazzaglia, A., Scala, A., Piperno, A., 2022. Linezolid nanoantiobiotics and sers-nanotags based on polymeric cyclodextrin bimetallic core-shell nanoarchitectures. Carbohydr. Polym. 293, 119736 https://doi.org/10.1016/j.carbpol.2022.119736.
Hu, H., Wang, H., Yang, Y., Xu, J.-F., Zhang, X., 2022. A bacteria-responsive porphyrin for adaptable photodynamic/photothermal therapy. Angew. Chem. Int. Ed. 61, e202200799.
Ikeda, A., Satake, S., Mae, T., Ueda, M., Sugikawa, K., Shigeto, H., Funabashi, H., Kuroda, A., 2017. Photodynamic activities of porphyrin derivative–cyclodextrin complexes by photoirradiation. ACS Med. Chem. Lett. 8, 555–559. https://doi.org/10.1021/acsmedchemlett.7b00098.
Judzewitsch, P.R., Corrigan, N., Wong, E.H.H., Boyer, C., 2021. Photo-enhanced antimicrobial activity of polymers containing an embedded photosensitiser. Angew. Chem. Int. Ed. 60, 24248–24256. https://doi.org/10.1002/anie.202110672.
Khurana, R., Kakatkar, A.S., Chatterjee, S., Barooah, N., Kunwar, A., Bhasikuttan, A.C., Mohanty, J., 2019. Supramolecular nanorods of (n-methylpyridyl) porphyrin with captisol: Effective photosensitizer for anti-bacterial and anti-tumor activities. Front. Chem. 7, 452. https://doi.org/10.3389/fchem.2019.00452.
Kirar, S., Thakur, N.S., Laha, J.K., Banerjee, U.C., 2019. Porphyrin functionalized gelatin nanoparticle-based biodegradable phototheranostics: Potential tools for antimicrobial photodynamic therapy. ACS Appl. Bio Mater. 2, 4202–4212. https://doi.org/10.1021/acsabm.9b00493.
Klausen, M., Ucuncu, M., Bradley, M., 2020. Design of photosensitizing agents for targeted antimicrobial photodynamic therapy. Molecules 25 (22), 5239.
Krishna, C.M., Uppuluri, S., Riesz, P., Jr, J.S.Z., Balasubramanian, D., 1991. A study of the photodynamic efficiencies of some eye lens constituents. Photochem. Photobiol. 54 (1), 51–58.
Mazzaglia, A., Micali, N., Villari, V., Zagami, R., Pennisi, R.M., Mellet, C.O., Fernández, J.M.G., Sciortino, M.T., Scolaro, L.M., 2017. A novel potential nanophototherapeutic based on the assembly of an amphiphilic cationic β-cyclodextrin and an anionic porphyrin. J. Porphyrins Phthalocyanines 21, 398–405. https://doi.org/10.1142/S108842461750033X.
Mineo, P., 2014. A porphyrin/β-cyclodextrin conjugated nano-system having a pan–lid molecular structure for smart drug carrier applications. Org. Biomol. Chem. 12, 3663–3670. https://doi.org/10.1039/C4OB00393D.
Mohanty, J., Bhasikuttan, A.C., Choudhury, S.D., Pal, H., 2008. Noncovalent interaction of 5,10,15,20-tetrakis(4-n-methylpyridyl)porphyrin with cucurbit[7]uril: A supramolecular architecture. J. Phys. Chem. B 112, 10782–10785. https://doi.org/10.1021/jp806012t.
Occhiuto, I.G., Castriciano, M.A., Trapani, M., Zagami, R., Romeo, A., Pasternack, R.F., Monsù Scolaro, L., 2020. Controlling j-aggregates formation and chirality induction through demetallation of a zinc(ii) water soluble porphyrin. Int. J. Mol. Sci. 21, 4001. https://doi.org/10.3390/ijms21114001.
Oyim, J., Omolo, C.A., Amuhaya, E.K., 2021. Photodynamic antimicrobial chemotherapy: Advancements in porphyrin-based photosensitize development. Front. Chem. 9, 635344 https://doi.org/10.3389/fchem.2021.635344.
Özkan, M., Kumar, Y., Keser, Y., Hadi, S.E., Tuncel, D., 2019. Cucurbit[7]uril-anchored porphyrin-based multifunctional molecular platform for photodynamic

antimicrobial and cancer therapy. ACS Appl. Bio Mater. 2, 4693–4697. https://doi.org/10.1021/acsabm.9b00763.
Pinto, S.C., Acunha, T.V., Santurio, J.M., Denardi, L.B., Iglesias, B.A., 2021. Investigation of powerful fungicidal activity of tetra-cationic platinum(ii) and palladium(ii) porphyrins by antimicrobial photodynamic therapy assays. Photodiagnosis Photodyn. Ther. 36, 102550 https://doi.org/10.1016/j.pdpdt.2021.102550.
Plenagl, N., Seitz, B.S., Reddy Pinnapireddy, S., Jedelská, J., Brüßler, J., Bakowsky, U., 2018. Hypericin loaded liposomes for anti-microbial photodynamic therapy of gram-positive bacteria. physica status solidi (a) 215, 1700837. https://doi.org/10.1002/pssa.201700837.
Redmond, R.W., Gamlin, J.N., 1999. A compilation of singlet oxygen yields from biologically relevant molecules. Photochem. Photobiol. 70, 391–475. https://doi.org/10.1111/j.1751-1097.1999.tb08240.x.
Romeo, A., Castriciano, M.A., Zagami, R., Pollicino, G., Monsù Scolaro, L., Pasternack, R. F., 2017. Effect of zinc cations on the kinetics of supramolecular assembly and the chirality of porphyrin j-aggregates. Chem. Sci. 8, 961–967. https://doi.org/10.1039/C6SC02686A.
Rubin Pedrazzo, A., Smarra, A., Caldera, F., Musso, G., Dhakar, N.K., Cecone, C., Hamedi, A., Corsi, I., Trotta, F., 2019. Eco-friendly β-cyclodextrin and linecaps polymers for the removal of heavy metals. Polymers (Basel) 11. https://doi.org/10.3390/polym11101658.
Sah, U., Sharma, K., Chaudhri, N., Sankar, M., Gopinath, P., 2018. Antimicrobial photodynamic therapy: Single-walled carbon nanotube (swcnt)-porphyrin conjugate for visible light mediated inactivation of staphylococcus aureus. Colloids Surf. B. Biointerfaces 162, 108–117. https://doi.org/10.1016/j.colsurfb.2017.11.046.
Santiago, P.S., Neto, D.d.S., Gandini, S.C.M., Tabak, M., 2008. On the localization of water-soluble porphyrins in micellar systems evaluated by static and time-resolved frequency-domain fluorescence techniques. Colloids Surf. B. Biointerfaces 65 (2), 247–256.
Seeger, M.G., Ries, A.S., Gressler, L.T., Botton, S.A., Iglesias, B.A., Cargnelutti, J.F., 2020. In vitro antimicrobial photodynamic therapy using tetra-cationic porphyrins against multidrug-resistant bacteria isolated from canine otitis. Photodiagnosis Photodyn. Ther. 32, 101982 https://doi.org/10.1016/j.pdpdt.2020.101982.
Shi, X., Zhang, C.Y., Gao, J., Wang, Z., 2019. Recent advances in photodynamic therapy for cancer and infectious diseases. Wiley Interdiscip. Rev. Nanomed. Nanobiotechnol. 11, e1560.
Simões, C., Gomes, M.C., Neves, M.G.P.M.S., Cunha, Â., Tomé, J.P.C., Tomé, A.C., Cavaleiro, J.A.S., Almeida, A., Faustino, M.A.F., 2016. Photodynamic inactivation of escherichia coli with cationic meso-tetraarylporphyrins – the charge number and charge distribution effects. Catal. Today 266, 197–204. https://doi.org/10.1016/j.cattod.2015.07.031.
Sortino, S., Mazzaglia, A., Monsù Scolaro, L., Marino Merlo, F., Valveri, V., Sciortino, M. T., 2006. Nanoparticles of cationic amphiphilic cyclodextrins entangling anionic porphyrins as carrier-sensitizer system in photodynamic cancer therapy. Biomaterials 27, 4256–4265. https://doi.org/10.1016/j.biomaterials.2006.03.035.
Swaminathan, S., Cavalli, R., Trotta, F., 2016. Cyclodextrin-based nanosponges: A versatile platform for cancer nanotherapeutics development. Wiley Interdiscip. Rev. Nanomed. Nanobiotechnol. 8, 579–601. https://doi.org/10.1002/wnan.1384.
Tian, J., Xia, L., Wu, J., Huang, B., Cao, H., Zhang, W., 2020. Linear alternating supramolecular photosensitizer for enhanced photodynamic therapy. ACS Appl. Mater. Interfaces 12, 32352–32359. https://doi.org/10.1021/acsami.0c07333.
Toledo, V.H., Yoshimura, T.M., Pereira, S.T., Castro, C.E., Ferreira, F.F., Ribeiro, M.S., Haddad, P.S., 2020. Methylene blue-covered superparamagnetic iron oxide nanoparticles combined with red light as a novel platform to fight non-local bacterial infections: A proof of concept study against escherichia coli. J. Photochem. Photobiol. B: Biol. 209, 111956 https://doi.org/10.1016/j.jphotobiol.2020.111956.
Trapani, M., De Luca, G., Romeo, A., Castriciano, M.A., Scolaro, L.M., 2017. Spectroscopic investigation on porphyrins nano-assemblies onto gold nanorods. Spectrochim. Acta A Mol. Biomol. Spectrosc. 173, 343–349. https://doi.org/10.1016/j.saa.2016.09.025.
Trapani, M., Mazzaglia, A., Piperno, A., Cordaro, A., Zagami, R., Castriciano, M.A., Romeo, A., Monsù Scolaro, L., 2020. Novel nanohybrids based on supramolecular assemblies of meso-tetrakis-(4-sulfonatophenyl) porphyrin j-aggregates and amine-functionalized carbon nanotubes. Nanomaterials 10, 669. https://doi.org/10.3390/nano10040669.
Trotta, F., Caldera, F., Cavalli, R., Soster, M., Riedo, C., Biasizzo, M., Uccello Barretta, G., Balzano, F., Brunella, V., 2016. Molecularly imprinted cyclodextrin nanosponges for the controlled delivery of l-dopa: Perspectives for the treatment of parkinson's disease. Expert Opin Drug Deliv 13, 1671–1680. https://doi.org/10.1080/17425247.2017.1248398.
Trotta, F., 2011. Cyclodextrin nanosponges and their applications, Cyclodextrins in pharmaceutics, cosmetics, and biomedicine, pp. 323-342.
Vera, C., Tulli, F., Borsarelli, C.D., 2021. Photosensitization with supramolecular arrays for enhanced antimicrobial photodynamic treatments. Front Bioeng Biotechnol 9, 655370. https://doi.org/10.3389/fbioe.2021.655370.
Wang, J., Liu, L., Chen, J., Deng, M., Feng, X., Chen, L., 2019. Supramolecular nanoplatforms via cyclodextrin host-guest recognition for synergistic gene-photodynamic therapy. Eur. Polym. J. 118, 222–230. https://doi.org/10.1016/j.eurpolymj.2019.04.051.
Wu, S., Xu, C., Zhu, Y., Zheng, L., Zhang, L., Hu, Y., Yu, B., Wang, Y., Xu, F.-J., 2021. Biofilm-sensitive photodynamic nanoparticles for enhanced penetration and antibacterial efficiency. Adv. Funct. Mater. 31, 2103591. https://doi.org/10.1002/adfm.202103591.
Wysocka-Król, K., Olsztyńska-Janus, S., Plesch, G., Plecenik, A., Podbielska, H., Bauer, J., 2018. Nano-silver modified silica particles in antibacterial photodynamic therapy. Appl. Surf. Sci. 461, 260–268. https://doi.org/10.1016/j.apsusc.2018.05.014.
Youf, R., Müller, M., Balasini, A., Thétiot, F., Müller, M., Hascoët, A., Jonas, U., Schönherr, H., Lemercier, G., Montier, T., Le Gall, T., 2021. Antimicrobial photodynamic therapy: Latest developments with a focus on combinatory strategies. Pharmaceutics 13 (12), 1995.
Zagami, R., Rapozzi, V., Piperno, A., Scala, A., Triolo, C., Trapani, M., Xodo, L.E., Monsù Scolaro, L., Mazzaglia, A., 2019. Folate-decorated amphiphilic cyclodextrins as cell-targeted nanophototherapeutics. Biomacromolecules 20, 2530–2544. https://doi.org/10.1021/acs.biomac.9b00306.
Zagami, R., Franco, D., Pipkin, J.D., Antle, V., De Plano, L., Patanè, S., Guglielmino, S., Monsù Scolaro, L., Mazzaglia, A., 2020. Sulfobutylether-β-cyclodextrin/5,10,15,20-tetrakis(1-methylpyridinium-4-yl)porphine nanoassemblies with sustained antimicrobial phototherapeutic action. Int. J. Pharm. 585, 119487 https://doi.org/10.1016/j.ijpharm.2020.119487.
Zhang, J., Yang, Z., Li, Y.-H., Durrani, S., Pang, A.-P., Gao, Y., Wu, F.-G., Lin, F., 2022. Super-stable chitosan-based nanoparticles for broad-spectrum antimicrobial photodynamic therapy. ACS Appl Polym Mater 4, 425–434. https://doi.org/10.1021/acsapm.1c01339.
Zheng, B.-D., Li, S.-L., Huang, Z.-L., Zhang, L., Liu, H., Zheng, B.-Y., Ke, M.-R., Huang, J.-D., 2020. A non-aggregated zinc(ii) phthalocyanine with hexadeca cations for antitumor and antibacterial photodynamic therapies. J. Photochem. Photobiol. B: Biol. 213, 112086 https://doi.org/10.1016/j.jphotobiol.2020.112086.